

TWO-EQUATION TURBULENCE MODELS FOR TURBINE BLADE HEAT TRANSFER SIMULATIONS

Jonas Larsson

jola@tfd.chalmers.se

Thermo and Fluid Dynamics

Chalmers University of Technology

S-412 96 Gothenburg, Sweden

A full Navier-Stokes solver is used to calculate external heat transfer in two linear two-dimensional turbine cascades, one subsonic and one transonic. A new nonlinear $k-\omega$ model is presented and compared with two classical low-Re $k-\epsilon$ models (Chien and Launder-Sharma) and two classical $k-\omega$ models (Wilcox standard and transition). The results are generally in good agreement with measurements, although the suction-side transition is not captured correctly by any model. All classical linear models over-predict the leading-edge heat transfer. This affects the $k-\epsilon$ models more than the $k-\omega$ models. The new nonlinear model works very well at the leading edge. The numerical quality of the results is discussed, and a few general guidelines about the numerics are given.

Nomenclature

C_p	Specific heat [J/kgK]
e_0	Total energy [J/kg]
k	Turbulent kinetic energy [J/kg]
p	Static pressure [Pa]
Pr	Prandtl number []
q_i	Heat flux [W/m ²]
t	Time [s]
T	Static temperature [K]
u_i	Velocity [m/s]
u^*	Friction velocity [m/s]
Y^+	Non-dim. distance from wall = $\frac{u^*y}{\nu}$ []
γ	Specific heat ratio = C_p/C_v []
ϵ	Dissipation of k [J/kg ³]
δ_{ij}	Kronecker's delta function []
μ	Dynamic viscosity [Ns/m ²]
ν	Kinematic viscosity [m ² /s]
ρ	Density [kg/m ³]
τ_{ij}	Shear stress tensor [N/m ²]
ω	Specific dissipation [s ⁻¹]

Subscripts

t Turbulent property

Superscripts

lam	Laminar part
tot	Laminar+turbulent part
$turb$	Turbulent part
"	Favre fluctuating part
$\bar{\cdot}$	Reynolds average
$\tilde{\cdot}$	Favre average

Copyright ©1997 by Jonas Larsson. Published by the American Institute of Aeronautics and Astronautics, Inc. with permission.

Introduction

The development of new gas turbines with high performance and improved efficiency often leads to increased cycle temperatures, higher mass-flows and lighter designs - trends which all tend to increase the heat-loads on the turbine blades. The temperature levels reached in the first stages of a modern gas turbine can cause mechanical problems and a decreased component life, and thereby limit the performance of the engine. Thus, turbine blade heat transfer is an important engineering problem. A numerical method which can predict the external heat transfer in the design phase would be a very valuable tool. This paper deals with one of the main difficulties in developing such a tool - to correctly model the influence of the turbulence on the flow and heat transfer.

The flow in a turbine is very complex. Large pressure gradients give strongly accelerated and decelerated regions. Under some operating conditions there might be separated regions. The gas entering the turbine comes from a combustor and is strongly turbulent. This increases the heat transfer in the laminar¹ and the turbulent parts^{2,3} of the boundary layers. It can also cause an earlier boundary layer transition. Shocks and shock-boundary layer interaction can trigger transition or separation and affect the heat transfer. Unsteady effects, caused by wakes and shocks from the preceding stages sweeping over the blades, can increase the heat transfer significantly⁴⁻⁶. In a real turbine secondary flows and 3D effects are also important⁷. Film cooling leads to even more complications, and will not be considered here.

Simplified methods like boundary layer solvers and Navier-Stokes solvers with algebraic turbulence models have been used by many researchers in the past to predict turbine heat transfer⁸⁻¹⁰. This can give good results for simple cases, but for cases with sepa-

rated regions, shocks and high turbulence levels these methods often have problems. By using a full Navier-Stokes solver with a transport turbulence model it is possible to account for history effects associated with the turbulence and thereby solve or reduce the problem encountered with other simpler methods.

In a previous paper¹¹ three low-Reynolds $k - \epsilon$ models and an algebraic model¹² were compared with turbine cascade heat transfer measurements. A following paper¹³, focusing on high inlet turbulence levels, extended the results to also cover linear $k - \omega$ models. In this paper, a new nonlinear $k - \omega$ model is developed and compared with measurements and results obtained with the more classical linear models.

All calculations presented here are for stationary and two-dimensional linear turbine cascades without cooling. This reduces the computational time and makes it possible to efficiently test different turbulence models. The test-cases chosen are a subsonic cascade by Nicholson et al.¹⁴, and a highly loaded transonic cascade¹⁵ from the von Karman Institute for Fluid Dynamics. Similar test cases which were also considered, can be found in the references^{16,17}.

Governing Equations

The governing equations are the Favre averaged¹⁸ continuity equation (1), momentum equation (2) and energy equation (3). Good overviews of the turbulent equations governing compressible flow can be found in the references^{19,20}. A detailed description of the main assumption underlying the equations as used here is available in the authors Licentiate thesis²¹. By assuming that the fluid is a perfect gas the pressure, \bar{p} , is given by (10).

The total shear stresses are expressed as a sum of the laminar and the turbulent contribution (4). The laminar part is given directly by (5), and the turbulent part is estimated with a separate turbulence model (see below). For the linear models this is done via an effective eddy-viscosity, μ_t , which according to the Boussinesq assumption gives the Reynolds stresses according to (6).

The heat-flux, q_i , is treated in a similar way, according to Reynolds analogy. First the heat-flux, q_i , is divided into a laminar and a turbulent part (7). The laminar part, q_i^{lam} , is given directly by (8). To model the turbulent heat-flux a constant turbulent Prandtl number, $Pr_t = 0.9$, is assumed, and (9) then gives an approximation of the heat-flux generated by turbulent fluctuations. The use of a constant turbulent Prandtl number is not self-evident. However, other researchers⁸ have reported no significant difference in heat transfer predictions when using an algebraic expression for the turbulent Prandtl number instead of a constant value.

It should be noted that for historical reasons the turbulent transport and molecular diffusion of turbu-

lent energy have been neglected in the energy equation (3). This does not influence the results at all for the subsonic and transonic cases presented here.

For simplicity the Favre ($\bar{\cdot}$) and Reynolds ($\overline{\cdot}$) averaging notation will be dropped in all subsequent sections.

$$\frac{\partial \bar{p}}{\partial t} + \frac{\partial}{\partial x_i} [\bar{\rho} \tilde{u}_i] = 0 \quad (1)$$

$$\frac{\partial}{\partial t} (\bar{\rho} \tilde{u}_i) + \frac{\partial}{\partial x_j} [\bar{\rho} \tilde{u}_j \tilde{u}_i + \bar{p} \delta_{ij} - \tau_{ij}^{tot}] = 0 \quad (2)$$

$$\frac{\partial}{\partial t} (\bar{\rho} \tilde{e}_0) + \frac{\partial}{\partial x_j} [\bar{\rho} \tilde{u}_j \tilde{e}_0 + \tilde{u}_j \bar{p} + \tilde{q}_j^{tot} - \tilde{u}_i \tau_{ij}^{tot}] = 0 \quad (3)$$

Where

$$\tau_{ij}^{tot} \stackrel{def}{=} \tau_{ij}^{lam} + \tau_{ij}^{turb} \quad (4)$$

$$\tau_{ij}^{lam} = \mu \left(\frac{\partial \tilde{u}_i}{\partial x_j} + \frac{\partial \tilde{u}_j}{\partial x_i} - \frac{2}{3} \frac{\partial \tilde{u}_k}{\partial x_k} \delta_{ij} \right) \quad (5)$$

$$\begin{aligned} \tau_{ij}^{turb} \stackrel{def}{=} -\overline{\rho u_i' u_j'} &\approx [\text{Linear Models}] \approx \\ &\approx \mu_t \left(\frac{\partial \tilde{u}_i}{\partial x_j} + \frac{\partial \tilde{u}_j}{\partial x_i} - \frac{2}{3} \frac{\partial \tilde{u}_k}{\partial x_k} \delta_{ij} \right) - \frac{2}{3} \bar{\rho} k \delta_{ij} \end{aligned} \quad (6)$$

$$\tilde{q}_j^{tot} \stackrel{def}{=} \tilde{q}_j^{lam} + \tilde{q}_j^{turb} \quad (7)$$

$$\tilde{q}_j^{lam} \approx -C_p \frac{\mu}{Pr} \frac{\partial \tilde{T}}{\partial x_j} = -\frac{\gamma}{\gamma - 1} \frac{\mu}{Pr} \frac{\partial}{\partial x_j} \left[\frac{\bar{p}}{\bar{\rho}} \right] \quad (8)$$

$$\begin{aligned} \tilde{q}_j^{turb} \stackrel{def}{=} C_p \overline{\rho u_j' T'} &\approx -C_p \frac{\mu_t}{Pr_t} \frac{\partial \tilde{T}}{\partial x_j} = \\ &= -\frac{\gamma}{\gamma - 1} \frac{\mu_t}{Pr_t} \frac{\partial}{\partial x_j} \left[\frac{\bar{p}}{\bar{\rho}} \right] \end{aligned} \quad (9)$$

$$\bar{p} = (\gamma - 1) \bar{\rho} \left(\tilde{e}_0 - \frac{\tilde{u}_k \tilde{u}_k}{2} - k \right) \quad (10)$$

Turbulence Models

The turbulence models used in this work are the low-Reynolds $k - \epsilon$ models of Chien²² and Launder-Sharma²³, and two linear $k - \omega$ models by Wilcox, one standard version²⁴ without any near-wall modifications, and one transition version²⁵, specifically optimized for transition simulations. Wilcox's book¹⁹ contains an exhaustive presentation of the $k - \omega$ models. A good review of classical low-Re $k - \epsilon$ models can be found in²⁶. These models were chosen in order to give a good representation of well established two-equation models. In addition to this a new nonlinear $k - \omega$ model is presented and tested.

None of the models used here were developed for compressible flow calculations. The only compressible modification used is that the turbulence equations are written in a conservative formulation. For the cases presented here this is sufficient.

All of the models were tested on simple flat-plate benchmark problems to assure a correct implementation before using them in cascade simulations.

$k - \epsilon$ Models

The low-Re $k - \epsilon$ models can be written in the general form of equation (11), (12), (13) and (14). C_{ϵ_1} , C_{ϵ_2} , C_μ , σ_k and σ_ϵ are model constants. The damping functions f_μ , f_1 and f_2 and the extra source terms D and E are only active close to solid walls and make it possible to solve k and ϵ down through the viscous sublayer. Table 1 summarizes the constants, damping functions and boundary conditions for all $k - \epsilon$ models used.

$$\frac{\partial}{\partial t}(\rho k) + \frac{\partial}{\partial x_j} \left[\rho k u_j - \left(\mu + \frac{\mu_t}{\sigma_k} \right) \frac{\partial k}{\partial x_j} \right] = P - \rho \epsilon - \rho D \quad (11)$$

$$\frac{\partial}{\partial t}(\rho \epsilon) + \frac{\partial}{\partial x_j} \left[\rho \epsilon u_j - \left(\mu + \frac{\mu_t}{\sigma_\epsilon} \right) \frac{\partial \epsilon}{\partial x_j} \right] = (C_{\epsilon_1} f_1 P - C_{\epsilon_2} f_2 \rho \epsilon) \frac{\epsilon}{k} + \rho E \quad (12)$$

$$\mu_t = C_\mu f_\mu \rho \frac{k^2}{\epsilon} \quad (13)$$

$$P = \tau_{ij}^{turb} \frac{\partial u_i}{\partial x_j} \quad (14)$$

	<i>Chien</i>	<i>Launder-Sharma</i>
c_μ	0.09	0.09
σ_k	1	1
σ_ϵ	1.3	1.3
D	$2\nu \frac{k}{y^2}$	$2\nu \left(\frac{\partial \sqrt{k}}{\partial y} \right)^2$
E	$-\frac{2\nu \epsilon}{y^2} e^{-0.5y^+}$	$2\nu \nu_t \left(\frac{\partial^2 u}{\partial y^2} \right)^2$
C_{ϵ_1}	1.35	1.44
C_{ϵ_2}	1.8	1.92
f_μ	$1 - e^{-0.0115y^+}$	$1 - e^{\frac{-3.4}{(1+Re_t/50)^2}}$
f_1	1	1
f_2	$1 - 0.22e^{-(\frac{Re_t}{6})^2}$	$1 - 0.3e^{-Re_t^2}$
$y^+ \stackrel{def}{=} \frac{yu^*}{\nu}$, $Re_t \stackrel{def}{=} \frac{k^2}{\nu \epsilon}$, $k_{wall} = 0$, $\epsilon_{wall} = 0$		

Table 1 Model Parameters, Low-Re $k - \epsilon$ Models

Linear $k - \omega$ Models

The linear $k - \omega$ models can be written in the general form of equation (15), (16), (17) and (18). The model parameters for the two models used are given in table 2.

$$\frac{\partial}{\partial t}(\rho k) + \frac{\partial}{\partial x_j} \left[\rho u_j k - (\mu + \sigma^* \mu_t) \frac{\partial k}{\partial x_j} \right] = P - \beta^* \rho \omega k \quad (15)$$

$$\frac{\partial}{\partial t}(\rho \omega) + \frac{\partial}{\partial x_j} \left[\rho u_j \omega - (\mu + \sigma \mu_t) \frac{\partial \omega}{\partial x_j} \right] = \alpha \frac{\omega}{k} P - \beta \rho \omega^2 \quad (16)$$

$$\mu_t = \alpha^* \frac{\rho k}{\omega} \quad (17)$$

$$P = \tau_{ij}^{turb} \frac{\partial u_i}{\partial x_j} \quad (18)$$

	<i>Standard Version</i>	<i>Transition Version</i>
α^*	1	$\frac{\alpha_0^+ + (Re_t/R_k)}{1 + (Re_t/R_k)}$
α	$\frac{5}{9}$	$\frac{5}{9} \cdot \frac{\alpha_0 + (Re_t/R_w)}{1 + (Re_t/R_w)} \cdot \frac{1}{\alpha^*}$
β^*	$\frac{9}{100}$	$\frac{9}{100} \cdot \frac{\frac{5}{18} + (Re_t/R_\beta)^4}{1 + (Re_t/R_\beta)^4}$
β	$\frac{3}{40}$	$\frac{3}{40}$
σ^*	$\frac{1}{2}$	$\frac{1}{2}$
σ	$\frac{1}{2}$	$\frac{1}{2}$
$Re_t \stackrel{def}{=} \frac{\rho k}{\omega \mu}$ $\alpha_0^* = \frac{\beta}{3}$ $\alpha_0 = \frac{1}{10}$		
$R_\beta = 8$ $R_k = 6$ $R_w = 2.7$		

Table 2 Model Parameters, Wilcox $k - \omega$ Models

The asymptotic behavior of ω approaching a wall is that $\omega \sim 1/y^2$ as $y \rightarrow 0$. However, using a finite value of ω_{wall} is good from a numerical point of view, and this is also what Wilcox recommends¹⁹. The surface roughness model gives a finite value for ω_{wall} as in equation (19) and (20). If k_R^+ , which is the non-dimensional average sand-grain roughness height, is set to a value below 5 a hydraulically smooth surface is obtained. If not otherwise stated, a k_R^+ value of 5 has been used in all simulations presented here. An investigation in a previous paper¹³ also showed that the heat transfer results are not sensitive to the value of k_R^+ as long as it is below 5. Using a very small value can cause numerical problems.

$$\omega_{wall} = \frac{u^{*2}}{\nu} S_R \quad (19)$$

Where

$$S_R = \begin{cases} (50/k_R^+) ^2 & k_R^+ < 25 \\ 100/k_R^+ & k_R^+ \geq 25 \end{cases} \quad k_R^+ \stackrel{def}{=} \frac{u^* k_R}{\nu} \quad (20)$$

Nonlinear $k - \omega$ Model

The nonlinear $k - \omega$ model is based on an algebraic stress-strain relation derived from Dimensional Analysis, Rapid Distortion Theory (RDT) and Realizability. The formulation used here was first proposed by Shih et al.^{27,28}. First dimensional analysis is used to obtain a truncated second order expression for the Reynolds stresses. This expression is then simplified using results from Rapid Distortion Theory^{29,30}. Realizability, defined as positiveness of all energy components and no violation of Schwarz' inequality between the fluctuating velocities, then gives further constraints on the model constants (29). A detailed derivation of this model can be found in²⁸. The final stress-strain relation is given by equation (26), where the turbulent times scale T is defined by (25) and the trace-less strain and rotation parameters are defined in (27) and (28). The two remaining constants A_0 and C_0 are tuned using homogeneous shear flow and surface flow in the inertial sublayer. The values used here (30) are the same as those proposed in²⁷.

In this work the nonlinear stress-strain relation is recast in a $k - \omega$ framework. This makes it possible to solve the equations down to the solid walls. The RDT technique used to derive the stress-strain relation is not strictly valid in the low-Reynolds number region. However, in a $k - \omega$ framework, the model performs reasonably well also in the inner parts of the boundary layers, and it has not been found necessary to use any further viscous corrections close to the walls. The same model constants as for the standard linear $k - \omega$ model are used with the nonlinear stress-strain relation.

$$\frac{\partial}{\partial t} (\rho k) + \frac{\partial}{\partial x_j} \left[\rho u_j k - (\mu + \sigma^* \mu_t) \frac{\partial k}{\partial x_j} \right] = P - \beta^* \rho \omega k \quad (21)$$

$$\frac{\partial}{\partial t} (\rho \omega) + \frac{\partial}{\partial x_j} \left[\rho u_j \omega - (\mu + \sigma \mu_t) \frac{\partial \omega}{\partial x_j} \right] = \alpha \frac{\omega}{k} P - \beta \rho \omega^2 \quad (22)$$

$$P \stackrel{def}{=} \tau_{ij}^{turb} \frac{\partial u_i}{\partial x_j} \quad (23)$$

$$\mu_t \stackrel{def}{=} C_\mu \rho k T \quad (24)$$

$$T \stackrel{def}{=} \frac{1}{\beta^* \omega} = \frac{k}{\epsilon} \quad (25)$$

$$\begin{aligned} \tau_{ij}^{turb} &\stackrel{def}{=} -\overline{\rho u_i' u_j'} \approx \\ &\approx -\frac{2}{3} \rho k \delta_{ij} + C_\mu \rho k 2 T S_{ij}^* - \\ &\quad - C_2 \rho k 2 T^2 (-S_{ik}^* \Omega_{kj}^* + \Omega_{ik}^* S_{kj}^*) \end{aligned} \quad (26)$$

$$\begin{aligned} S_{ij}^* &\stackrel{def}{=} S_{ij} - \frac{1}{3} S_{kk} \delta_{ij} & S_{ij} &\stackrel{def}{=} \frac{1}{2} \left(\frac{\partial u_i}{\partial x_j} + \frac{\partial u_j}{\partial x_i} \right) \\ \Omega_{ij}^* &\stackrel{def}{=} \Omega_{ij} & \Omega_{ij} &\stackrel{def}{=} \frac{1}{2} \left(\frac{\partial u_i}{\partial x_j} - \frac{\partial u_j}{\partial x_i} \right) \end{aligned} \quad (27)$$

$$\begin{aligned} U^* &\stackrel{def}{=} \sqrt{S_{ij}^* S_{ij}^* + \Omega_{ij}^* \Omega_{ij}^*} & S^* &\stackrel{def}{=} \sqrt{S_{ij}^* S_{ij}^*} \\ \Omega^* &\stackrel{def}{=} \sqrt{\Omega_{ij}^* \Omega_{ij}^*} & W^* &\stackrel{def}{=} \frac{S_{ij}^* S_{jk}^* S_{ki}^*}{(S^*)^3} \end{aligned} \quad (28)$$

$$\begin{aligned} C_\mu &= \frac{1}{A_0 + A_s^* U^* T} & C_2 &= \frac{\sqrt{1 - (3C_\mu S^* T)^2}}{C_0 + 6S^* \Omega^* T^2} \\ A_s^* &= \sqrt{6} \cos \phi_1 & \phi_1 &= \frac{1}{3} \arccos \sqrt{6} W^* \end{aligned} \quad (29)$$

$$A_0 = 6.5 \quad C_0 = 1.0 \quad (30)$$

Numerical Method

The Navier-Stokes solver used in this work is based on the G2DFLOW³¹ series of codes developed by L.-E. Eriksson at Volvo Aero Corporation. The code uses an explicit three-stage Runge-Kutta time-marching scheme with an optimized local time-step for stationary simulations. The grid is a structured multi-block grid which is generated with transfinite interpolation. The convective (Euler) parts are discretized with a third order accurate cell-centered finite volume reconstruction scheme with upwind-biasing based on the characteristic variables and associated velocities. For the turbulent quantities (k and ϵ/ω), which are very source term dominated and sensitive to over-shots, it is necessary to add an extra TVD limiter to this scheme, making it second order accurate. The viscous parts are discretized with a compact second order scheme.

The use of an explicit method and a local time-step makes it difficult to solve k and ϵ/ω . Stability problems often occur at the beginning of a simulation, and it might be necessary to temporarily limit the turbulent viscosity, use a first order upwind scheme for k and ϵ/ω or limit the time-step locally to avoid too large relative cell-updates. After a few thousand time-steps all of these modifications can be removed. All results presented here are without any extra limiters on the turbulent quantities and with a second order accurate TVD scheme for k and ϵ/ω .

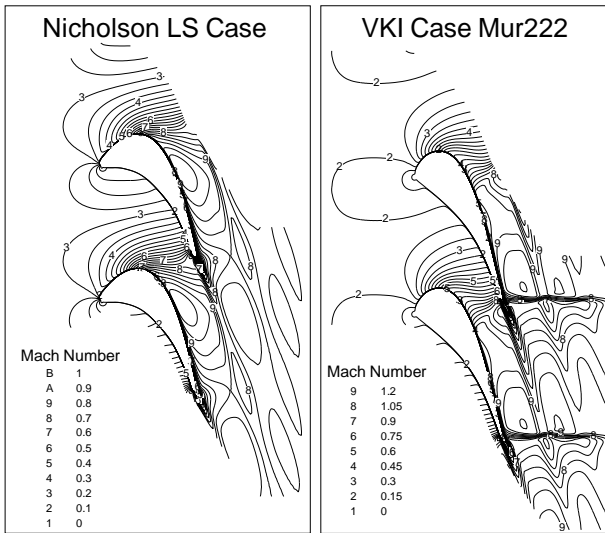


Fig. 1 Mach Number Contours

The boundary condition at the inlet and outlet are of the simplest absorbing type. That means that the same upwind-biased characteristic reconstruction scheme, which is used in the domain, is used at the inlet and outlet boundaries. At the blade surface the flow variables are mirrored to ghost-cells outside the domain to get the correct conditions at the wall.

A more thorough description of the numerical methods can be found in²¹.

Simulations

The test-cases are a subsonic cascade by Nicholson et. al.¹⁴, and a highly loaded transonic cascade¹⁵ from the von Karman Institute for Fluid Dynamics. Exact specification of inlet and outlet conditions and geometrical data can be found in the references. There is no information about the turbulent length scale ($L = k^{1.5}/\epsilon = \sqrt{k}/(\beta^*\omega)$) at the inlet for the two cases. A length scale corresponding to 10% of the pitch was used for all simulations presented here. Using a different length-scale does not influence the results very much.

The characteristics of the flow in the two cascades can be seen from the Mach number plots in figure 1. All turbulence model give the same pressure and Mach number distributions for the two cases. Hence, different heat transfer results are not caused by different global flow fields, but are a result of details in the boundary layers and the turbulent fields.

Subsonic Cascade

Heat transfer measurement for this cascade, referred to as the “low-staggered (LS)” cascade, have been published by Nicholson et al.¹⁴. The operating conditions used here is the high turbulence level (4%) at design flow-rate, which gives a maximum Mach number just below 1 and a Reynolds number based on exit velocity and chord of $1.113 \cdot 10^6$. The boundary layer on the suction is laminar to about 30% of the axial length, where

transition starts. The transition region is quite long, and from about 60% of the axial length the boundary layer is fully turbulent. On the pressure side transition occurs close to the leading edge, and the boundary layer remains in a turbulent state over the whole blade. The acceleration at the rear of the blade does not cause any relaminarization.

The low turbulence ($< 0.2\%$) version of this case was used in a previous paper¹¹. The conclusion was that an algebraic turbulence model (Baldwin-Lomax) gives very good results, and that it is not necessary to us a transport model. But to model the influence of a higher inlet turbulence level only transport models are used for the high turbulence level case presented here.

Figure 2 and 3 shows heat transfer results obtained with different $k-\epsilon$ models and $k-\omega$ models.

All linear models over-predict the production of turbulent energy in stagnation regions, and this gives rise to a large peak in the heat transfer at the leading edge of the blade. The $k-\epsilon$ models are more affected by this than the $k-\omega$ models. This is because the ϵ equation tends to convect too large length scales into the boundary layers in stagnation flows. Of the $k-\epsilon$ models used here the Chien model is most affected by this. In a previous paper¹¹ it was shown that adding an extra Yap³² source term to the ϵ equation, which drives the length scale to its equilibrium value, reduces these problems, and improves the results when using the Chien model. One way to remove the excessive production of turbulent energy around the leading edge is to modify the production term by replacing the square of the strain with a product of strain and vorticity. This modification, originally suggested by Kato and Launder³³, were also tested, and was found to give too low heat transfer predictions in the leading edge region. The results were nearly laminar. The Kato-Launder modification also deteriorated the results in other regions. A physically more sound and better approach is to use a nonlinear stress-strain relation. The nonlinear model used here also significantly improves the results at the leading edge. The heat transfer at the leading edge is captured almost exactly. It should be noted that the leading edge heat transfer in this case is influenced by the inlet turbulence level and that this effect is modeled correctly by the nonlinear turbulence model.

Only the Launder-Sharma model is able to capture the laminar region on the suction side. All other models give an almost immediate transition and fully turbulent results for the entire suction side. However, the transition obtained with the Launder-Sharma model is too early and too abrupt. It is not influenced by the inlet turbulence level or length scale, neither is it influenced by the excessive production of turbulent energy at the leading edge. This is contrary to the physics of the flow and indicates that the by-pass transition is not modeled correctly. The same problem has also been observed by other authors³⁴ for the same case

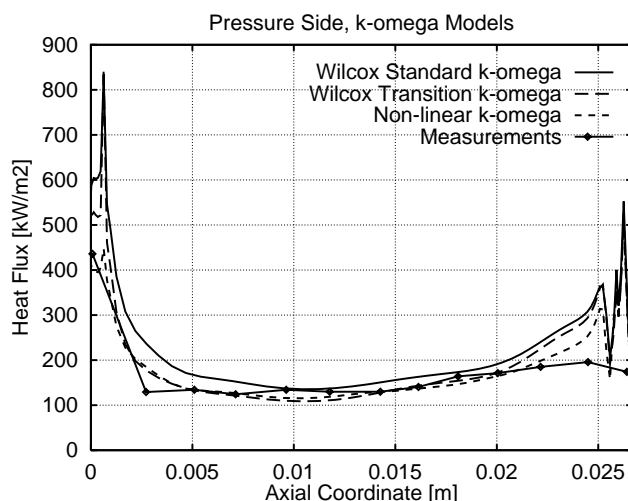
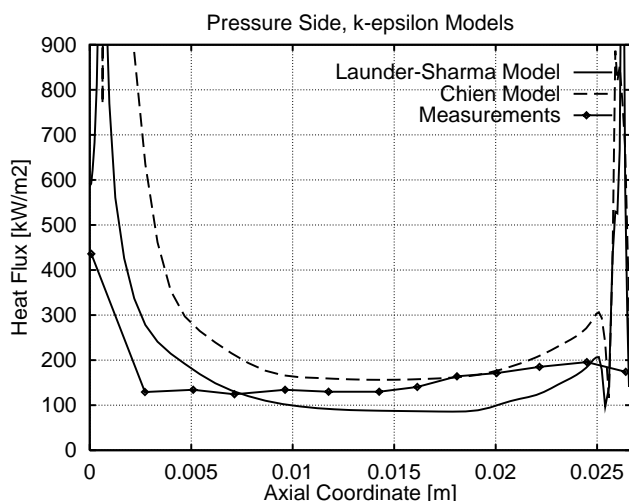
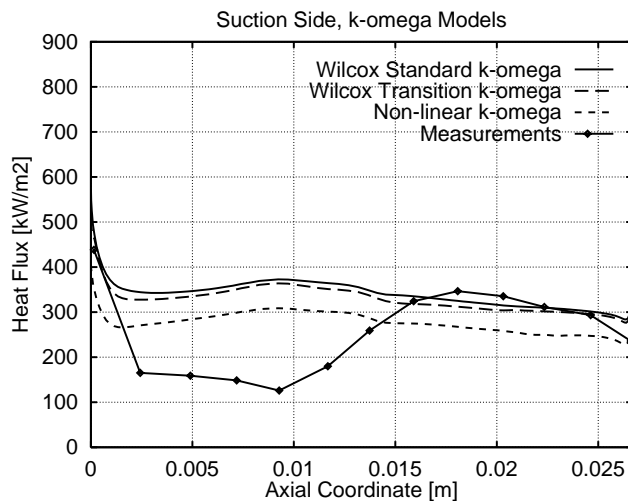
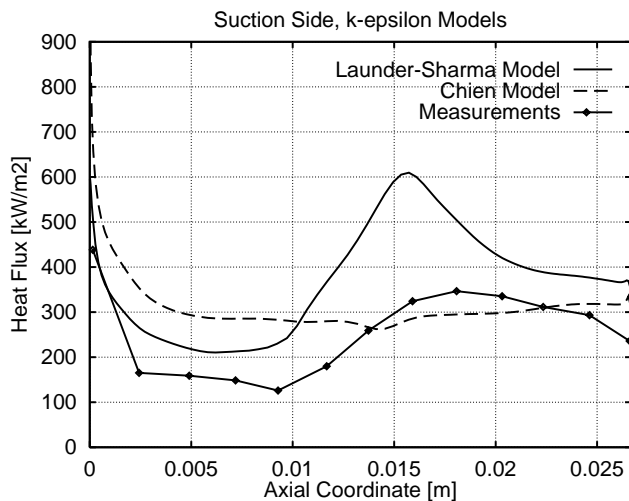


Fig. 2 Heat Transfer, $k - \epsilon$, Subsonic LS Case

Fig. 3 Heat Transfer, $k - \omega$, Subsonic LS Case

using the Launder-Sharma model and a new nonlinear three equation model. They also did simulations at different Reynolds number, and not even then did the transition point move. For the case presented here the transition seems to be determined by the global flow and the geometry. In the turbulent region on the suction side all models give good results.

The pressure side is predicted well by all models. The $k - \omega$ models are slightly better than the $k - \epsilon$ models. The decrease in heat transfer close to the trailing edge is not captured well with any model. There is a strong acceleration of the flow in this region, and the laminarizing effect of this is probably not modeled correctly. The nonlinear model performs slightly better than the other models in this region.

$k - \omega$ models are often too sensitive to the inlet value of ω . In lack of a good transition model this can be used to tune the simulations to get the correct transition point³⁵. Attempts to do this for this case failed. The results presented here are not very sensitive to the inlet ω value.

Transonic Cascade

The second test-case is a transonic highly loaded cascade from the von Karman Institute of Fluid Dynamics (VKI). Heat transfer measurements at different operating conditions are available in Arts et al.¹⁵. The case chosen here is referred to as Mur222. It has a high inlet turbulence level of 6%, an outlet Mach number of 1.1, and a chord Reynolds number based on outlet conditions of $5 \cdot 10^5$. This is a difficult case to simulate with a two equation model since large parts of the boundary layers are not fully turbulent. On the suction side the boundary layer remains in a laminarizing state all the way back to the shock, which is located just at the trailing edge. Also on the pressure side the boundary layer is laminarizing, and no transition is visible.

Figure 4 and 5 shows heat-transfer results obtained with $k - \epsilon$ and $k - \omega$ models.

Again all linear models over-predict the heat transfer at the leading edge. The problem is not so severe for this case because it has a very blunt nose. The nonlinear $k - \omega$ model predicts the heat transfer at the leading edge very well.

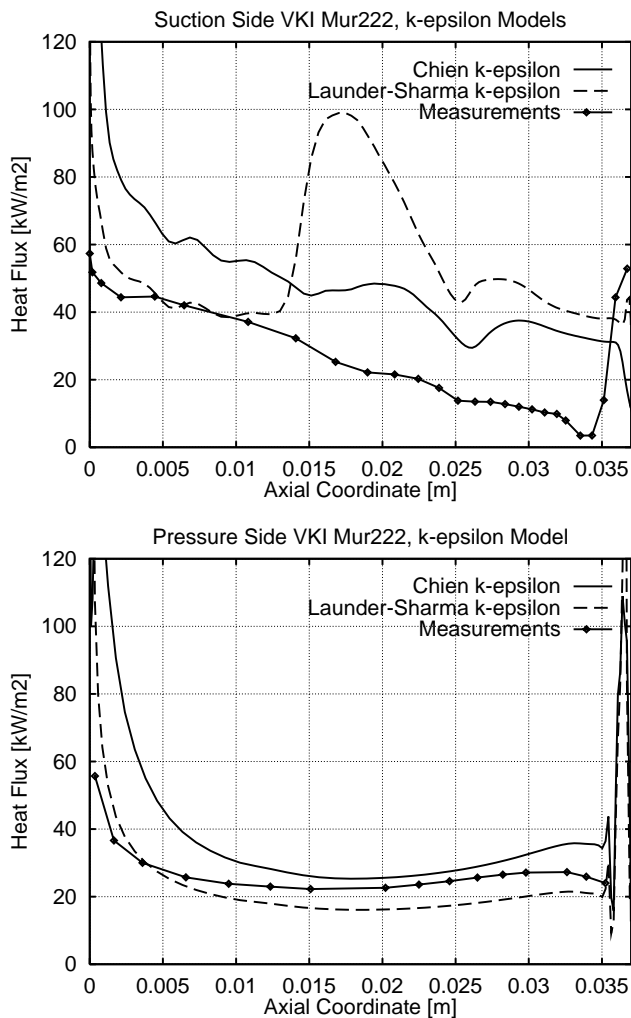


Fig. 4 Heat Transfer, $k - \epsilon$, Transonic VKI Case

Also for this case the Launder-Sharma model is the only model that gives any laminar region on the suction side. The transition is too early, and has the same characteristic peak as seen previously. With the other models the results on the suction side are fully turbulent. It should be noted that the effect of the fish-tail shock/expansion wave is predicted well and has the correct location, although the absolute level is not correct.

On the pressure side the $k - \epsilon$ models agree well with the measurements. The $k - \omega$ models over-predict the heat-transfer slightly. The general trend is captured well by all models, although they predict a too strong increase in the heat-transfer close to the trailing edge. Again the nonlinear model performs better in this region than the linear models.

Numerical Errors

When working with CFD and advanced turbulence models it is essential to have good control of the numerical errors. Especially the heat transfer is very sensitive to small errors. A lot of effort has been put into ensuring that all simulation presented here are

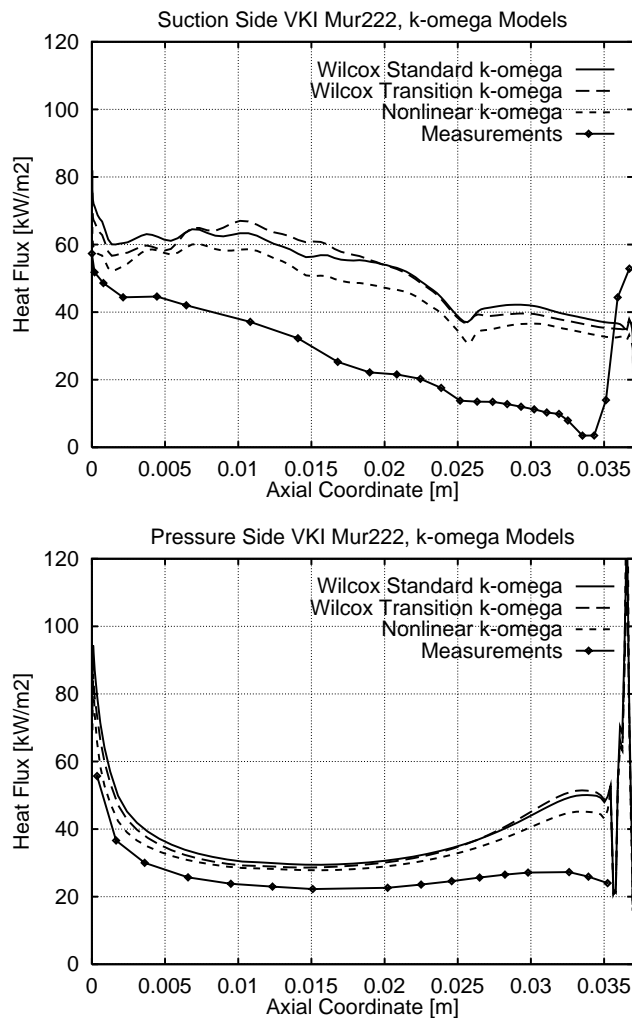


Fig. 5 Heat Transfer, $k - \omega$, Transonic VKI Case

of good numerical quality, and that the results are representative of the turbulence models and not the numerics.

All results have been verified to be grid independent. Almost exactly the same results were obtained using two different grids, one fine grid and one coarse grid with half as many cells. The fine grid has approximately 20.000 nodes for both cases. The resolution of the boundary layers has also been investigated. This was done by varying Y^+ for the first row of cells closest to the wall. The author recommends using a Y^+ below 0.2 everywhere. A Y^+ below 1.0 is usually sufficient to get correct results, but using a Y^+ below 0.2 reduces problems with oscillations and improves stability, and thus makes it easier to obtain a converged solution.

It is often necessary to use double precision. The damping functions used in many low-Reynolds models are sensitive to truncation errors, and using single precision can causes problems sometimes. All simulations presented here were done in double precision.

The $k - \omega$ models generally cause less numerical problems than the $k - \epsilon$ models. The reason for this is not well understood. Put it is probably related to the

more stable boundary condition on ω .

For heat transfer simulations it is extra important to be careful when generating the grid. Using third order interpolating splines often gives oscillations and a surface which is not completely smooth. This usually does not affect the pressure distribution, but it immediately leads to oscillations in the heat transfer. Using 5:th ordered smoothed splines solves this problem.

The thermal field and the heat transfer converges much slower than the velocity and pressure fields. It is not sufficient to use a common density variation criteria to determine convergence. The best criteria is usually to plot the heat transfer, run a few thousand time steps more, and plot it again to see if it has changed. This technique was used for all cases presented here.

Conclusions

All the linear models, which are based on the Boussinesq assumption, predict far too high turbulence levels in the stagnation region. The $k - \epsilon$ models, and especially the Chien model, are more influenced by this than the $k - \omega$ models, and give a large peak in the heat transfer. The $k - \omega$ models are only affected in a very small region around the stagnation point.

The new nonlinear $k - \omega$ gives very good results in the leading edge region, and appears to be able to correctly model the influence of a higher inlet turbulence level.

None of the models used predict the suction side transition correctly. Only the Launder-Sharma model gives a significant laminar region. However, the transition point is not influenced by the free-stream turbulence or the excessive production of turbulent energy in the leading edge region. The transition, contrary to physics, is governed by the flow and the local blade geometry, and not by the external turbulence.

The heat transfer in the turbulent part of the suction-side is predicted well by all models, although the Launder-Sharma model over-predicts it slightly.

The heat transfer on the pressure side is also predicted well, except near the trailing edge where there sometimes is an unphysical rise in the heat-transfer. The nonlinear model is a bit better than the other models in this region, although the results are not very good. The Launder-Sharma model has a tendency to under-predict the pressure side heat-transfer slightly.

It is important that the numerical quality of the solution is verified in some way. All models can give converged but incorrect results if the resolution of the boundary-layers is not sufficient.

The $k - \omega$ models are easier to use numerically than the $k - \epsilon$ models, and their results are as good or better. The $k - \omega$ models also work better, but not well, in the leading edge region. No major difference has been found between the standard and the transition version of the $k - \omega$ model. To get good results in the leading

edge region it is necessary to use a nonlinear model. The new nonlinear $k - \omega$ model gives good results, and is easy to use. It does not cause any additional numerical difficulties.

Acknowledgment

Professor Lars-Erik Eriksson at Volvo Aero Corporation helped with the numerical parts of the project. Professor Ulf Häll has been supervising the work at Chalmers since 1994.

This research project is funded by the Swedish National Space Board and Volvo Aero Corporation. It is part of a cooperation between Chalmers University of Technology (CTH), Volvo Aero Corporation (VAC), Ecole Central de Lyon (ECL) and Société Européenne de Propulsion (SEP) to develop new methods to predict turbine blade heat transfer.

References

- ¹Dullenkopf, K. and Mayle, R. E., "The Effect of a Incident Turbulence and Moving Wakes on Laminar Heat Transfer in Gas Turbines," *ASME Journal of Turbomachinery*, Vol. 116, No. 1, 1994, pp. 23-28.
- ²Thole, K. A. and Bogard, D. G., "Enhanced Heat Transfer due to High Free-Stream Turbulence," *ASME Journal of Turbomachinery*, Vol. 117, 1995, pp. 418-424.
- ³Maciejewski, P. K. and Moffat, R. J., "Heat Transfer With Very High Free-Stream Turbulence: Part I and II," *ASME Journal of Heat Transfer*, Vol. 114, 1992, pp. 827-839.
- ⁴Dullenkopf, K., Schultz, A., and Wittig, S., "The Effect of a Incident Wake Conditions on the Mean Heat Transfer of an Airfoil," *ASME Journal of Turbomachinery*, Vol. 113, 1991, pp. 412-418.
- ⁵Magari, P. J. and LaGraff, L. E., "Wake-Induced Unsteady Stagnation-Region Heat Transfer Measurements," *ASME Journal of Turbomachinery*, Vol. 116, No. 1, 1994, pp. 29-38.
- ⁶Rao, K. V., Delaney, R. A., and Dunn, M. G., "Vane-Blade Interaction in a Transonic Turbine," *Journal of Propulsion and Power*, Vol. 10, No. 3, 1994, pp. 305-317.
- ⁷Blair, M. F., "An Experimental Study of Heat Transfer in a Large-Scale Turbine Rotor Passage," *ASME Journal of Turbomachinery*, Vol. 116, No. 1, 1994, pp. 1-13.
- ⁸Boyle, R. J., "Navier-Stokes Analysis of Turbine Blade Heat Transfer," *ASME Journal of Turbomachinery*, Vol. 113, No. 3, 1991, pp. 392-403.
- ⁹Ameri, A. A., Sockol, P. M., and Gorla, R. S. R., "Navier-Stokes Analysis of Turbomachinery Blade External Heat Transfer," *Journal of Propulsion and Power*, Vol. 8, No. 2, 1992, pp. 374-381.
- ¹⁰Daniels, L. D. and Browne, W. B., "Calculation of Heat Transfer Rates to Gas Turbine Blades," *International Journal of Heat and Mass Transfer*, Vol. 24, No. 5, 1981, pp. 871-879.
- ¹¹Larsson, J., Eriksson, L.-E., and Häll, U., "External Heat Transfer Predictions in Supersonics Turbines Using the Reynolds Averaged Navier-Stokes Equations," *Proc. 12:th IS-ABE Conference, Melbourne*, Vol. 2, (Copies distributed by AIAA), September 1995, pp. 1102-1112.
- ¹²Baldwin, B. S. and Lomax, H., "Thin Layer Approximation and Algebraic Model for Separated Turbulent Flows," *AIAA Paper 78-257*, 1978.
- ¹³Larsson, J., "Turbine Blade Heat Transfer Calculations Using Two-Equation Turbulence Models," *Proc. 2:nd European Conference on Turbomachinery Fluid Dynamics and Thermodynamics, Antwerpen, Belgium*, March 1997, pp. 411-420.

- ¹⁴Nicholson, J. H., Forest, A. E., Oldfield, M. L. G., and Schultz, D. L., "Heat Transfer Optimised Turbine Rotor Blades - An Experimental Study Using Transient Techniques," ASME Paper 82-GT-304, 1982.
- ¹⁵Arts, T., Lambert de Rouvriot, M., and Rutherford, A. W., "Aero-Thermal Investigation of a Highly Loaded Transonic Liner Turbine Guide Vane Cascade," Tech. Rep. 174, von Karman Institute for Fluid Dynamics, 1990.
- ¹⁶Hylton, L. D., Mihelc, M. S., Turner, E. R., Nealy, D. A., and York, R. E., "Analytical and Experimental Evaluation of the Heat Transfer Distribution Over the Surfaces of Turbine Vanes," NASA CR-168015, 1983.
- ¹⁷Yeh, F. C., Hippensteele, S. A., Van Fossen, J. G., and Poinsatte, P. E., "High Reynolds Number Turbulence Effects on Turbine Heat Transfer," *Journal of Propulsion and Power*, Vol. 10, No. 6, 1994, pp. 868-875.
- ¹⁸Favre, A., "Equations des Gaz Turbulents Compressibles," *Journal de Mecanique*, Vol. 4, No. 3, 1965, pp. 361-390.
- ¹⁹Wilcox, D. C., *Turbulence Modeling for CFD*, DCW Industries, Inc., La Cañada, California, 1993.
- ²⁰Vandromme, D., "Turbulence modeling for Compressible Flows and Implementation in Navier-Stokes Solvers," von Karman Institute for Fluid Dynamics, Lecture Series 1991-02, Introduction to the Modeling of Turbulence, 1991.
- ²¹Larsson, J., "Numerical Simulation of Turbine Blade Heat Transfer," Licentiate Thesis, Department of Thermo and Fluid Dynamics, Chalmers University of Technology, Gothenburg, Sweden (Also available on the Internet at <http://www.tfd.chalmers.se/~jola/>), 1996.
- ²²Chien, K.-Y., "Predictions of Channel and Boundary-Layer Flows with a Low-Reynolds Number Turbulence Model," *AIAA Journal*, Vol. 20, No. 1, 1982, pp. 33-38.
- ²³Launder, B. E. and Sharma, B. I., "Application of the Energy-Dissipation Model of Turbulence to the Calculation of Flow Near a Spinning Disc," *Letters in Heat and Mass Transfer*, Vol. 1, No. 2, 1974, pp. 131-138.
- ²⁴Wilcox, D. C., "Reassessment of the Scale Determining Equation for Advanced Turbulence Models," *AIAA Journal*, Vol. 26, No. 11, 1988, pp. 1299-1310.
- ²⁵Wilcox, D. C., "Simulation of Transition with a Two-Equation Turbulence Model," *AIAA Journal*, Vol. 32, No. 2, 1994, pp. 247-255.
- ²⁶Patel, V. C., Rodi, W., and Scheuerer, G., "Turbulence Models for Near-Wall and Low Reynolds Number Flows: A Review," *AIAA Journal*, Vol. 23, No. 9, 1985, pp. 1308-1319.
- ²⁷Shih, T.-H., "Chapter 4, One Point Turbulence Closures," *Proc. ERCOFTA/IUTAM Summer School on Turbulence and Transition Modelling, Stockholm*, June 1995, pp. 4.1-4.36.
- ²⁸Shih, T.-H., Zhu, J., and Lumley, J. L., "A New Reynolds Stress Algebraic Equation Model," NASA TM-106644, 1994.
- ²⁹Reynolds, W. C., "Fundamentals of Turbulence for Turbulence Modeling and Simulation," Lecture Notes, von Karman Institute for Fluid Dynamics, also AGARD-CP-93, NATO, 1987.
- ³⁰Mansour, N. N., Shih, T.-H., and Reynolds, W. C., "The Effect of Rotation on Initially Anisotropic Homogenous Flow," *Physics of Fluids A*, Vol. 3, 1991, pp. 2421-2425.
- ³¹Eriksson, L.-E., "Development and Validation of Highly Modular Flow Solver Versions in G2DFLOW and G3DFLOW Series for Compressible Viscous Reacting Flow," Tech. Rep. 9970-1162, Volvo Aero Corporation, Trollhättan, Sweden, 1995.
- ³²Yap, C. J., *Turbulent Heat and Momentum Transfer in Recirculating and Impinging Flows*, Ph.D. thesis, Faculty of Technology, University of Manchester, 1987.
- ³³Kato, M. and Launder, B. E., "The Modeling of Turbulent Flow Around Stationary and Vibrating Square Cylinders," *Proc. 9th Symposium on Turbulent Shear Flows, Kyoto*, August 1993, pp. 10.4.1-10.4.6.
- ³⁴Craft, T. J., Launder, B. E., and Suga, K., "The Prediction of Turbulent Transitional Phenomena with a Non-Linear Eddy Viscosity Model," *Proc. of the Engineering Foundation International Conference on Turbulent Heat Transfer, San Diego*, March 1996.
- ³⁵Chima, R. V., "A $k-\omega$ Turbulence Model for Quasi-Three-Dimensional Turbomachinery Flows," AIAA Paper 96-0248 and NASA TM-107051, 1996.